SANDIA REPORT

SAND87—0696 • UC—62a
Unlimited Release
Printed December 1987

Thermal Fatigue of Stainless Steel

W. B. Jones, R. J. Bourcier, J. A. Van Den Avyle

Prepared by
Sandia National Laboratories
Albuquerque, New Mexico 87185 and Livermore, California 94550
for the United States Department of Energy
under Contract DE-AC04-76DP00789

Issued by Sandia National Laboratories, operated for the United States Department of Energy by Sandia Corporation.

Printed in the United States of America
Available from
National Technical Information Service
U.S. Department of Commerce
5285 Port Royal Road
Springfield, VA 22161

NTIS price codes
Printed copy: A03
Microfiche copy: A01

Distribution
Category UC-62a

SAND 87-0696

Unlimited Distribution
Printed December 1987

THERMAL FATIGUE OF STAINLESS STEEL

W. B. Jones, R. J. Bourcier, and J. A. Van Den Avyle

Sandia National Laboratories
Albuquerque, NM 87185

Abstract

Two austenitic steels, 316 Stainless Steel and Alloy 800, have been examined under conditions of both isothermal low cycle fatigue (LCF) and thermomechanical fatigue (TMF). The TMF tests were conducted between 649 and 360°C with a carefully controlled triangular waveform. The LCF tests were performed at 649°C and both kinds of tests were subjected to a strain range of 0.5%. TMF shortened life to 40% for 316 Stainless Steel and to 5% for Alloy 800. The microstructural evolution occurring in both alloys has been examined and we conclude these do not play a role in the life shortening caused by TMF. The TMF does produce asymmetric hysteresis loops with large tensile peak stresses in tests where the maximum temperature corresponded with the peak compressive stress. The influence of TMF on fatigue crack growth rates has been measured and it was found that TMF accelerated crack growth in Alloy 800 and slowed it down slightly in 316 Stainless Steel. The dominant influence of TMF appears to be in fatigue crack initiation, with the tensile peak stress development driving early crack initiation.

TABLE OF CONTENTS

FIGURES

Introduction

Thermomechanically induced fatigue is an important part in the service conditions present in structures used at elevated temperatures. This includes tube and piping components of stainless steel used in such energy conversion technologies as nuclear reactors, fossil fueled power plants, and solar central receiver plants. In the first two applications, the number of thermal cycles is purposely kept small to minimize the damaging effects of the thermomechanical cycles; in the third case the diurnal solar cycles and cloud passage make this impossible. The current baseline service condition established for central receiver design is 10,000 cycles accumulation in 30 years plant lifetime. Thermomechanical fatigue (TMF) effects are present in all of these applications but contribute differently in each one depending on how much cycling occurs during service.

Given the difficulty of performing thermomechanical cycling tests, it is not surprising that few thorough studies have been conducted. Some testing has involved moving samples between baths or furnaces maintained at two different temperatures or by using a programmable controller to drive a furnace. Such testing is limited in that direct comparisons to the isothermal low cycle fatigue data base are difficult. References 1, 2, and 3 describe several typical earlier studies.

Both 316 Stainless Steel and Alloy 800 are austenitic alloys commonly used in elevated temperature applications. The 316 Stainless Steel contains 13% Ni and 17% Cr with 2% Mo for added high temperature strength; Alloy 800 is an iron based alloy containing 33% Ni and 21% Cr and was developed to have good corrosion resistance. The higher Cr content also makes this alloy more resistant to sensitization than 316 Stainless Steel making Alloy 800 desirable in welded structures. The strength, fatigue and creep properties of Alloy 800 are at least comparable to the 300 series stainless steels properties (4), leading to use of Alloy 800 as a tubing and piping alloy in nuclear reactors and solar receivers as an alternative to the 300 series stainless steels. In fact, the low strain range isothermal low cycle fatigue (LCF) lifetime data for Alloy 800 are significantly longer than for 316 Stainless Steel (5, 6). Metallurgical studies of Alloy 800 (7-10) have shown that the microstructural evolution of this alloy is more complex and is less well understood than is 316 Stainless Steel (11, 12). This complexity comes primarily from the presence of Aℓ and Ti in Alloy 800. These elements may be present (by ASTM specification) at up to 0.6% and can give rise to significant amounts of TiC carbides and γ' ($Ni_3(A\ell,Ti)$) precipitates. There is a competition for the carbon (<0.10% specified) between the two stable carbides, $M_{23}C_6$ and TiC and the extent of TiC formation determines how much (Aℓ + Ti) would be available for subsequent γ' precipitation. In addition, final volume fractions of these phases have been shown to be history sensitive (13, 8, 9, 10) with variations in both chemistry and processing history influencing the microstructural evolution and mechanical properties during elevated temperature testing or service. Austenite decomposition in 316 Stainless Steel has been studied and found to constitute only $M_{23}C_6$ carbide precipitation for up to about 103 hours of exposure at 650°C (11, 12).

The ASME Boiler and Pressure Vessel Code and Code Case N-47 which are used to design the stainless steel piping components for these applications do not explicitly treat TMF effects. However, the current rules in N-47 incorporate an important assumption of material behavior: that isothermal cycling at the peak temperature is a conservative estimate of fatigue lifetime under thermomechanical cycling conditions. This is incorporated through the use of strain controlled LCF data to determine the baseline fatigue curves included in N-47. The correctness of this assumption is not critical to the design of fossil fueled plants or nuclear reactors since the alloy performance there reflects predominantly the creep or cyclic creep behaviors. For the solar application, the thermal cycling aspects of material response must be treated correctly. The appropriate way to treat this effect in structural design is not the topic of this paper. Rather, the purpose of this study was to carefully test this assumption and examine the strengthening and fatigue crack growth mechanisms present during TMF.

Experimental Procedure

Starting Materials

Table 1 shows the chemistries of the heats of 316 Stainless Steel and Alloy 800 used in this study; both are fully within the ASTM specifications for those alloys. In addition to the different chromium and nickel contents between the two alloys, several other differences are significant. The 316 Stainless Steel contains about 2% Mo as a solid solution strengthener at elevated temperature which Alloy 800 does not have. The Alloy 800 contains 0.4% each of Ti and Aℓ which are not present in the 316 Stainless Steel.

Table 1 - Alloy Compositions, Weight Percent

	Fe	Cr	Ni	Mo	Mn	C	Ti	Aℓ	Si
316 Stainless(1)	bal	17.2	13.5	2.34	1.86	.057	.02	--	.58
Alloy 800 (2)	46.5	20.0	31.0	--	--	.04	.40	.40	.24

(1) Oak Ridge National Laboratory Reference Heat No. 8092297
(2) Produced by Huntington Alloy Products Division of International Nickel Corp. (Heat HH 8989A)

Optical metallography of the two alloys is shown in Figure 1. The primary difference seen at this scale is grain size: 5 to 15 μm for the Alloy 800, and about 75 μm for the 316 Stainless Steel. The 316 Stainless Steel starting structure reflects the solution anneal treatment (about 1 hour at 1180°C) given this alloy. Transmission electron microscopy (TEM) has shown that essentially all of the carbides have been dissolved and the dislocation density was very low. The Alloy 800 material shows extensive $M_{23}C_6$ carbide precipitation in both optical microscopy and TEM. An earlier

study (9) of this heat of Alloy 800 describes the starting condition in more detail. These particles lie along current grain boundaries as well as in arrays which are suggestive of precipitation along prior grain boundaries. A fine distribution (10 to 100 nm particles) of TiC carbides was found in the form of linear arrays which probably mark the location of prior twin boundaries. This alloy received the standard final mill anneal treatment of one hour at 1000°C. This results in recrystallization of the austenitic matrix without dissolution of most of the carbide particles already present.

Mechanical Testing

The tests performed in this study were done on a 245 kN MTS servo-hydraulic test system. The basic test configuration is shown in Figure 2. The test specimen used in this study is axisymmetric (gage 6.35 mm dia. X 12.7 mm length) with button grip ends. Water-cooled split collet grips are

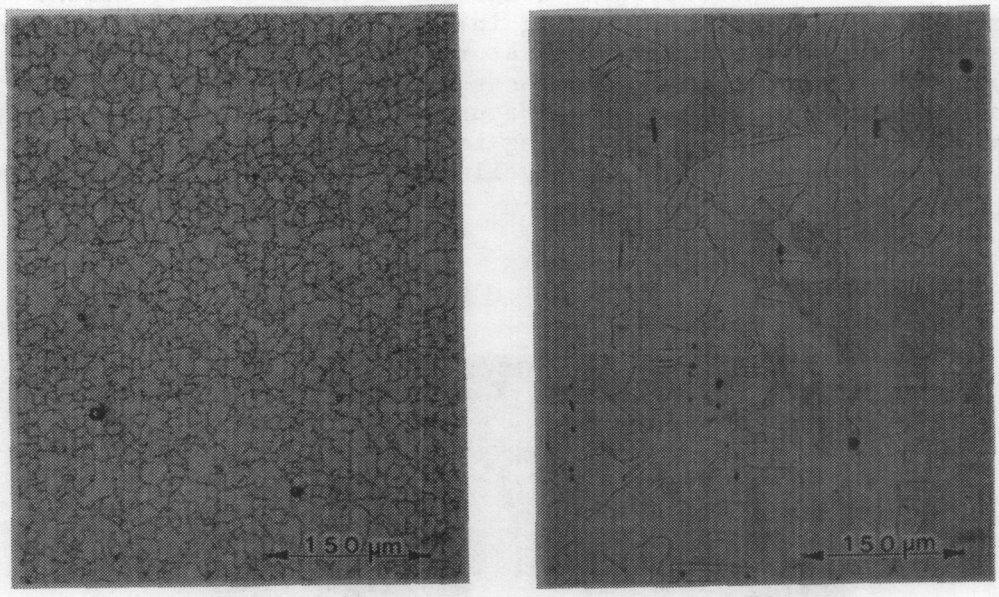

Figure 1. Optical microstructures of (a) Alloy 800 and (b) 316 Stainless Steel.

used to provide good axial alignment during fully reversed loading. Specimen heating is accomplished with a 7.5 kW Lepel RF generator using a water cooled copper coil to give a temperature gradient of less than 5°C over the specimen gage length. Temperature is monitored using either K-type thermocouples or a Vanzetti infrared optical pyrometry system. Strain is measured using a water cooled MTS quartz rod axial extensometer. For tests utilizing the optical pyrometry system, the specimen is painted with a flat black coating (Pyromark) which allows efficient radiation of infrared energy from the specimen surface (emissivity = 0.93).

LCF tests were performed using an MTS 410 digital function generator to provide a triangular waveform for total strain control. The TMF tests were carried out using a computer controlled test system described in detail elsewhere (14). Briefly, the system uses a DEC PDP 11/34 computer for data acquisition and test control through an MTS 433 interface to an MTS 442 controller. Specimen temperature is monitored with the optical pyrometry system and controlled by varying power to the RF generator through a Leeds & Northrup Electromax V digital temperature controller and/or activating a forced air cooling system. All programs used for test control and data acquisition are written in MTS MultiUser Basic. This computer control allows simultaneous ramping of strain and temperature, which enables both in-phase and out-of-phase TMF testing to be accurately performed. The triangular thermal cycle followed the control signal very closely with no resolvable overshoot at either temperature peak.

LCF tests were performed at a fully reversed total strain range of 0.5% at 649°C for cyclic periods of 10 and 60 seconds. In the interest of clarity, we will introduce the following nomenclature to define thermomechanical cycling: testing in which the compressive stress peak coincides with the maximum temperature will be designated as HTC (High-Temperature-Compression) while tests in which the tensile stress peak coincides with the maximum temperature will be designated as HTT (High-Temperature-Tension). HTC cycling is simply performed by maintaining a fixed specimen gage length and cycling temperature between the upper and

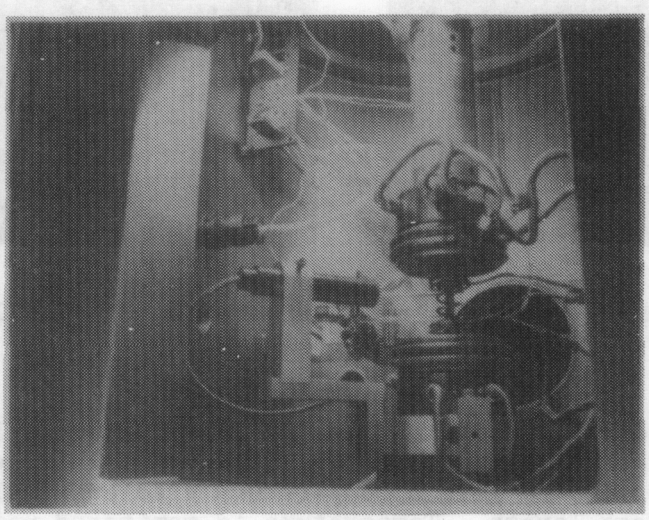

Figure 2. Testing configuration.

lower limits selected to yield the desired level of thermal expansion strain. HTT cycling, on the other hand, requires that the specimen gage be extended and compressed in phase by twice the amount which accompanies simple free thermal expansion. A temperature range of 360 to 649°C was used in the TMF tests, which were performed at 0.5% strain range for cyclic periods of 60 seconds. HTC TMF tests were performed on Alloy 800 which incorporated either tensile or compressive hold times of 5 minutes.

A concern which should be addressed concerning TMF test technique is the effect of forced air cooling on thermal stress development within our test specimen. The question is whether or not preferential cooling of the specimen surface causes enhanced tensile stresses, resulting in premature crack initiation. The thermal diffusivity and thermal conductivity of both alloys are approximately 4.1 mm^2/s and 5.1 cal/s•m•°C, respectively, over the temperature range of interest. We assume convective cooling of a semi-infinite rod (15) to approximate our 6.25 mm diameter specimens from 649°C to 375°C in 30 s (our infrared pyrometry readings should be true surface measurements). The Fourier number for this test specimen is 12.6, which at a relative temperature of 0.52 (400°C surface temperature) corresponds to a Biot number of 0.02-0.05. The resulting temperature difference from center to surface is negligible - certainly not large enough to have a significant effect on surface stresses.

Microstructural Examination

Transmission electron microscopy was used to characterize the substructures of both alloys. Transverse slices about 0.5 mm thick were cut from the gage sections of the fatigue specimens using a low speed saw. Disks 3 mm in diameter were cut from these slices by electrical discharge machining. Individual disks ground to about 0.1 mm thickness were polished to perforation with a twin jet electropolisher. The electrolyte used was a solution of 10% perchloric acid and 90% methanol held at <-40°C. The foils were examined in a JEM 200CX operated at 100 kV. Finer precipitates (<100 nm in diameter) were generally distinguished by dark field microscopy and selected area diffraction was used to crystallographically identify the phases.

Fractography

Fracture surfaces examined in the scanning electron microscope were first coated with gold-palladium by vacuum sputtering to eliminate charging effects caused by oxides which formed at elevated temperatures. For fatigue striation spacing measurements, surfaces were carefully oriented normal to the electron beam, and micrographs were taken at crack length intervals measured by the stage micrometer. Average striation spacings at a crack length were determined by counting the number of striations along a line length on the micrographs. Several measurements were taken on each micrograph, and these were averaged to gain the overall average.

Results

Mechanical Testing

Cyclic Hardening. The cyclic hardening of 316 Stainless Steel and Alloy 800 are summarized in Figures 3 through 7. The isothermal cyclic hardening response of both materials is nearly identical, showing roughly balanced cyclic stress peaks throughout the tests and saturation in stress range early in the tests. Decreasing strain rate for 316 Stainless Steel results in an expanded stress range during initial cycling (Figure 3). By 100 cycles, this difference has essentially disappeared and the two tests nearly overlay for most of the test duration.

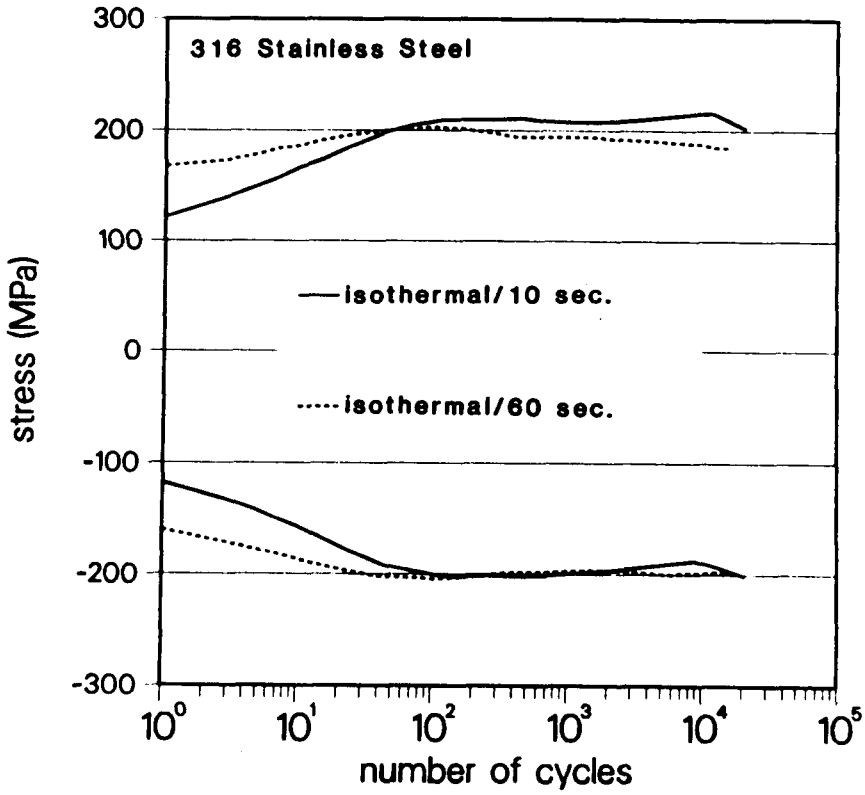

Figure 3. Cyclic hardening of 316 Stainless Steel in isothermal fatigue, 649°C, $\Delta\epsilon$=0.5%.

For Alloy 800, virtually no difference is observed in the initial isothermal cyclic hardening response for the two strain rates examined. At approximately 1000 cycles, however, the slower test (Figure 4) shows stress saturation and subsequent strain softening, while the faster test continues to slightly harden to failure.

A major difference in the cyclic hardening response of these two alloys appears during TMF testing. Under thermomechanical cycling, 316 Stainless Steel displays a hardening response which is qualitatively similar to that it shows during isothermal testing (Figure 5). In both cases, cyclic stress

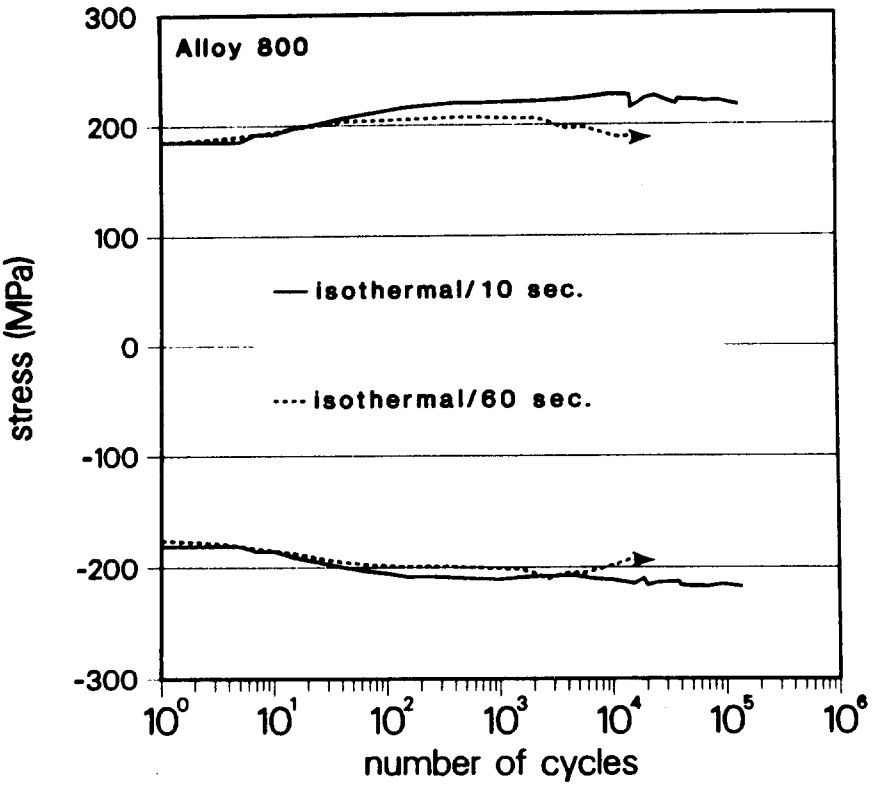

Figure 4. Cyclic hardening of Alloy 800 in isothermal fatigue, 649°C, $\Delta\epsilon$=0.5%.

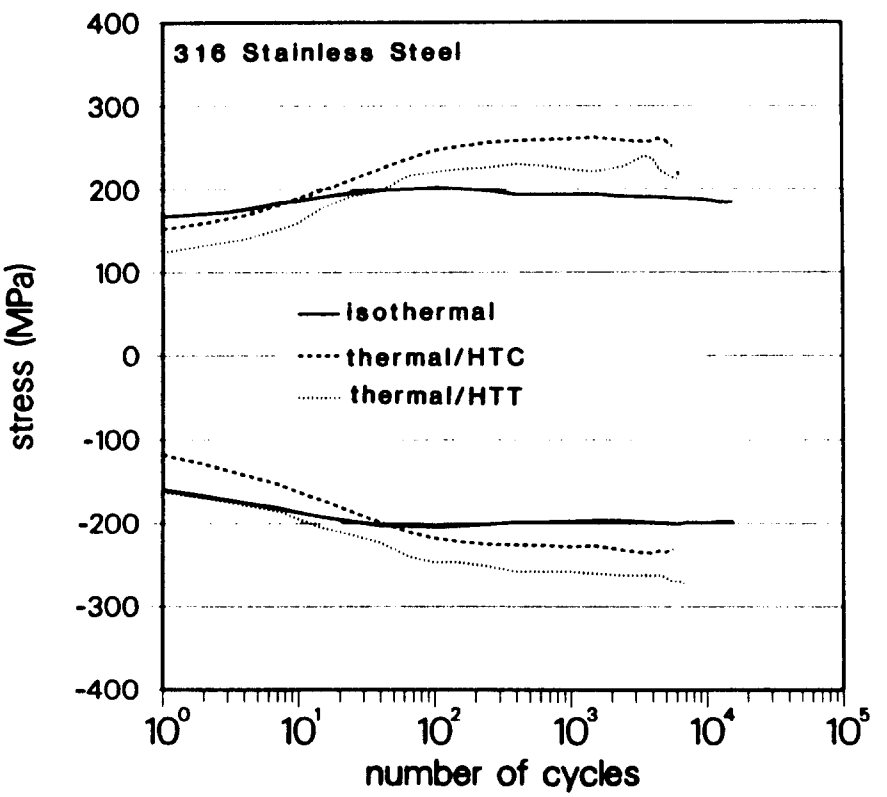

Figure 5. Cyclic hardening of 316 Stainless Steel in thermomechanical fatigue.

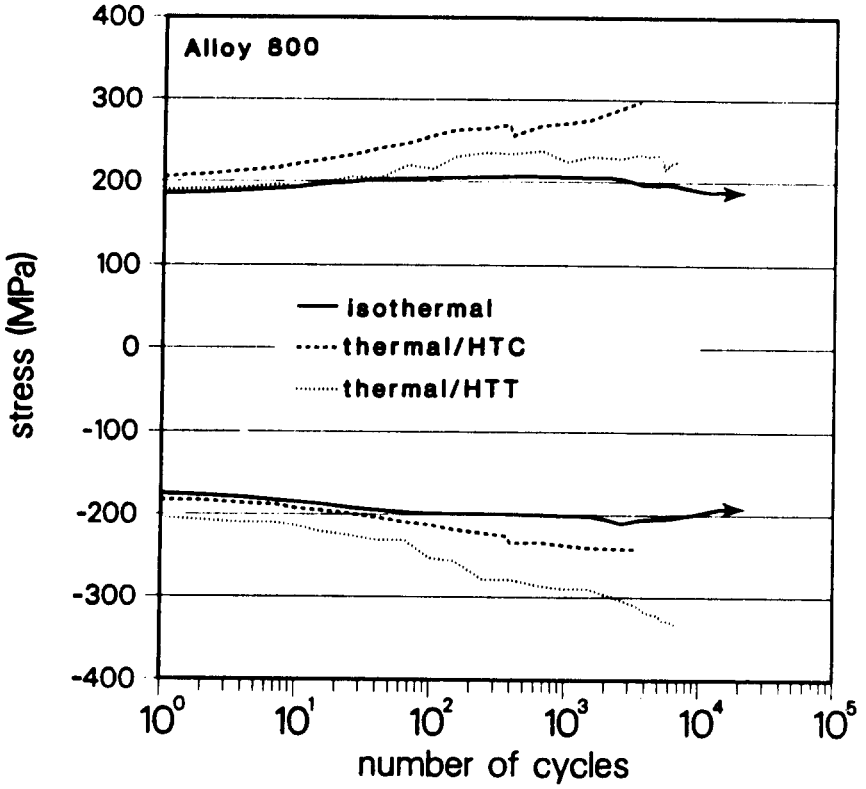

Figure 6. Cyclic hardening of Alloy 800 in thermomechanical fatigue.

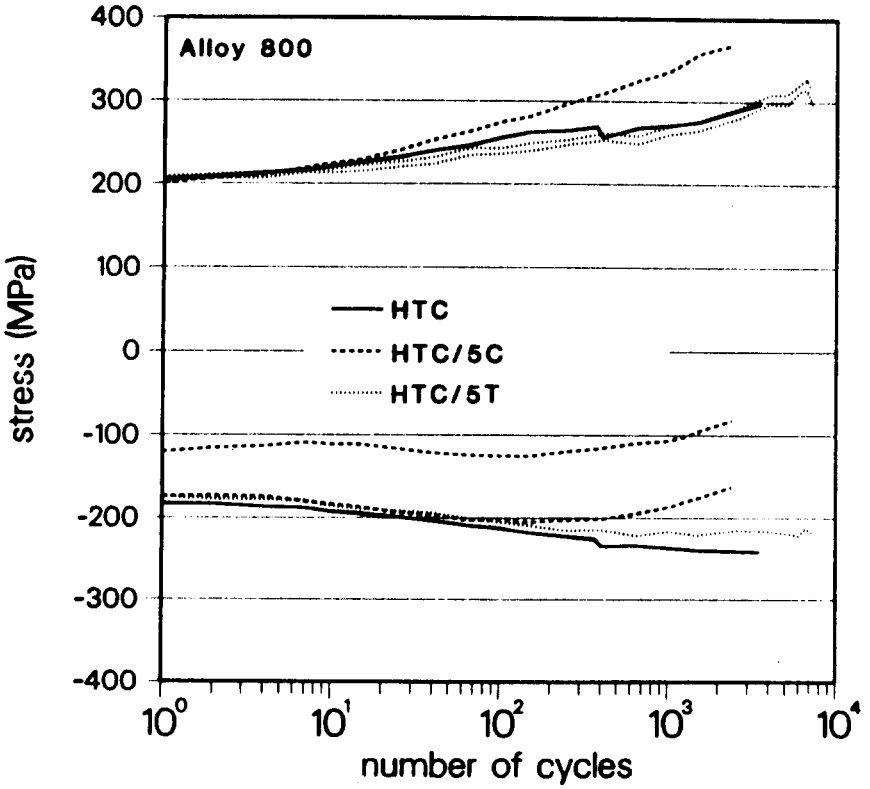

Figure 7. Cyclic hardening of Alloy 800 in thermomechanical fatigue with hold periods.

peak saturation is reached in about 100 cycles. However, the total stress range during thermomechanical cycling is about 25% larger than in isothermal tests. Stress peaks in both tension and compression are increased, with the largest difference occurring on the low temperature side of the cycle; the result is the development of 20-30 MPa mean stresses during TMF.

In contrast, the TMF cyclic hardening response of Alloy 800 is qualitatively unlike that developed for isothermal testing. The stress peak histories are distinctly asymmetric in shape, with no stress peak saturation on the low temperature side of the cycle. Again the stress peak histories are asymmetric in shape, resulting in the development of roughly 30 MPa mean stresses (Figure 6). These mean stresses are the result of low temperature stress peaks which are approximately 60 MPa higher than observed in isothermal testing, while the high temperature stress peak is essentially coincident with that observed in isothermal testing. Incorporation of a five minute compressive hold period during HTC cycling (Figure 7) results in significantly enhanced tensile mean stress development ($\simeq$100 MPa) while a five minute tensile hold yields results which are virtually indistinguishable from the continuous cycling test.

Table 2 - Plastic Strain Ranges in Isothermal and Thermomechanical Tests.

Material	Test Type	Dep (%)
316 Stainless	isothermal, 649°C	0.25
316 Stainless	thermal/HTC	0.19
Alloy 800	isothermal, 649°C	0.25
Alloy 800	thermal/HTC	0.15
Alloy 800	thermal/HTC/5C	0.13
Alloy 800	thermal/HTC/5T	0.13

Measurements of plastic strain range in the TMF tests were made at the zero stress values of the stress-temperature hysteresis loops. At zero stress, the difference in temperatures on opposite sides of the loop cause a thermal strain which is purely plastic ($\alpha\Delta T = \Delta\sigma/E = 0$). Measured values are given in Table 2. Since stress ranges for the TMF tests are higher than for the isothermal tests, the elastic strain ranges are necessarily greater. With equal total strain ranges, the plastic strain ranges for the TMF tests are significantly lower than for the isothermal tests.

Fatigue Life. The number of cycles to failure for the specimens examined in this study are listed in Table 3, where all results are for 0.5% total strain range. The cyclic life of 316 Stainless Steel was found to be moderately sensitive to both strain rate and thermomechanical history over the range of strain rate/temperature examined here. In isothermal cycling, increasing the cycle time by a factor of six (from 10 to 60 s) decreases the fatigue life to 75%. For the same 60 second cycle time, TMF cycling has a more dramatic effect - a reduction in life to 40%. Interestingly, this decrease in life is similar for both the HTC and HTT thermomechanical cycles.

Table 3 - Summary of Cycles to Failure, 0.5% Total Strain Range

Material	Test Type	Strain Rate (s-1)	Cycles to Failure
316	isothermal, 649°C	0.0010	22000 (2)
316	isothermal, 649°C	0.00017	16700 (1)
316	thermal/HTC	0.00017	5600 (3)
316	thermal/HTT	0.00017	6900 (2)
800	isothermal, 649°C	0.0010	116000 (4)
800	isothermal, 649°C	0.00017	>15900
800	thermal/HTC	0.00017	5700 (2)
800	thermal/HTC/5C	0.00017	2400 (2)
800	thermal/HTC/5T	0.00017	7300 (1)
800	thermal/HTT	0.00017	6900 (2)

( ) - Number of specimens tested for each condition

Alloy 800 displays an much stronger effect of TMF. The cyclic lives of specimens thermomechanically fatigued at 60 s/cycle are only about 5% of the average value of samples isothermally fatigued at 10 s/cycle at 649°C. The fraction of this life reduction due to rate sensitivity was not completely established, but an isothermal test using the slower 60 s/cycle time was run to 15900 cycles without any evidence of impending failure. This is significantly longer than any of the TMF tests. Samples cycled with HTC thermomechanical cycles and 5 minute compressive hold periods (5C) show the shortest cyclic lives.

Comparing the two alloys, the LCF cyclic life of Alloy 800 is about 5 times that of 316 stainless; the lives measured here agree well with published compilations (5, 6). TMF cycles to failure are nearly equal for HTC cycling of the two alloys.

Microstructural Observations

316 Stainless Steel. Isothermal cycling at 0.5% strain range and 649°C produces the changes from the solution annealed structure shown in Figure 8 which contrasts with the nearly dislocation free microstructure of the starting condition. This strain range produces a highly heterogeneous dislocation substructure with most regions near grain boundaries having developed a cell structure with cell sizes of about 1 μm. In some areas, these cells are narrow and well ordered while in other areas the walls are more loosely knit. The centers of almost all grains, and the whole of some grains, did not develop a cellular dislocation structure.

Both intergranular and transgranular precipitation of $M_{23}C_6$ occurred during this test which lasted only 36 hours. Carbides formed intergranularly in the form of blocky, 0.1 to 0.2 μm particles which have formed in sufficient density to be nearly continuous along the boundaries. Also present was a dispersion of very fine (<50 nm) carbide particles distributed throughout the substructure.

The substructure developed during thermomechanical cycling is shown in Figure 9. The dislocation structure produced in this test was similar in character to that formed isothermally with differences in only the volume fraction of cellular structure. Most cells which did form were not well developed and were about 1 μm in size.

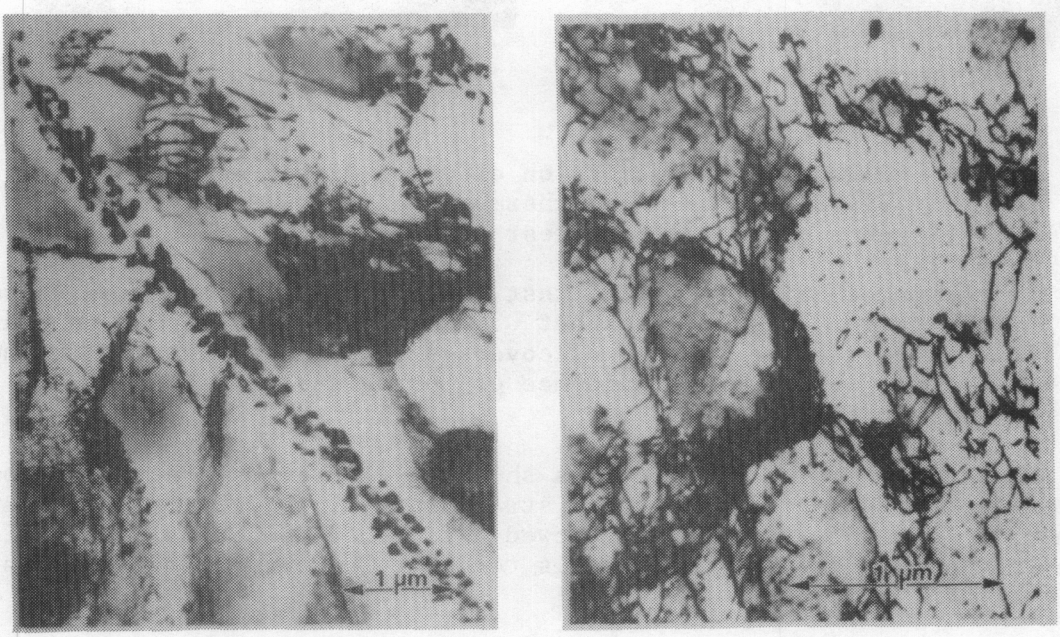

(a) (b)

Figure 8. Transmission electron micrographs of 316 Stainless Steel isothermally fatigue cycled at 649°C, 6 s/cycle, 36 hr. test duration.

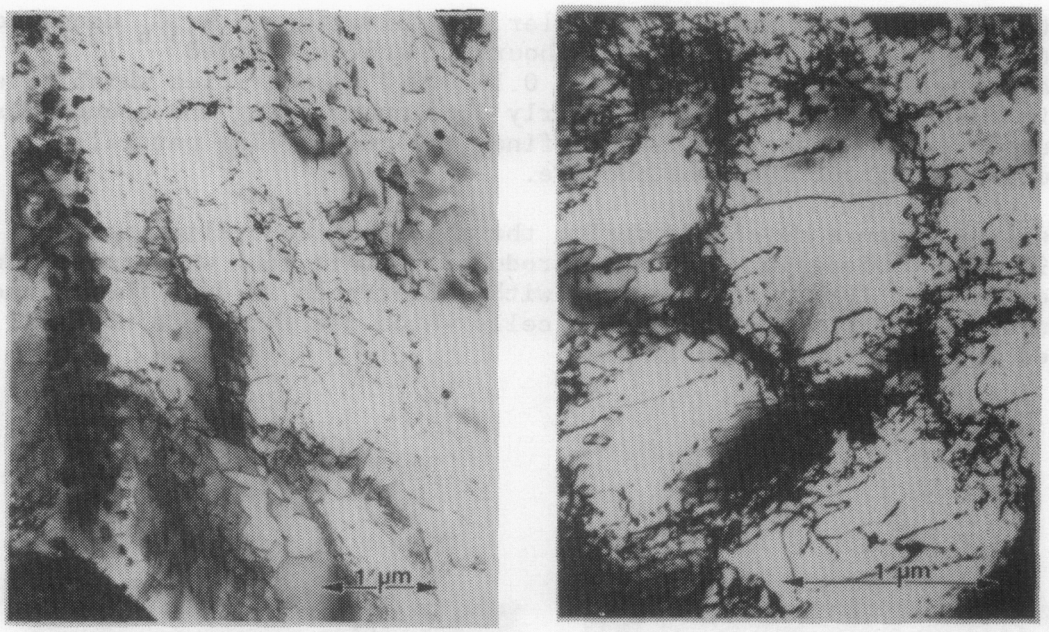

Figure 9. Transmission electron micrographs of 316 Stainless Steel thermomechanical HTC cycled, 60 s/cycle, 117 hr. test duration.

The thermomechanically cycled test lasted 117 hours and also showed $M_{23}C_6$ precipitation. Particles about 0.1 μm in size had formed on grain and twin boundaries with the density of coverage lower than observed in the isothermal test. We found no evidence of intragranular carbide precipitation in this TMF test.

Alloy 800. The microstructures shown in Figure 10 were taken from an isothermal test conducted at a slow strain rate of 1.7×10^{-4} s-1 and run for 270 hours. Much of the material showed a tendency toward cell formation. Where they were observed, these cells tended to be several micrometers in size.

The $M_{23}C_6$ carbide was present in the starting material and continued precipitation had occurred during testing. In addition to the idiomorphic 0.5 - 1.0 μm particles already present, our examination showed intergranular precipitation of blocky particles 0.1-0.2 μm in size. Also present was a very fine dispersion of $M_{23}C_6$ particles shown in Figure 10a.

The sample of continuous cycling TMF examined was in test for only 75 hours which is reflected in the substructure. Figure 11 shows that no additional $M_{23}C_6$ precipitation was observed. We found clear evidence of cell formation although it was not extensive and these cells ranged in size

from 1- 2 μm. The cell formation was more extensive in the thermomechanically cycled specimen than in the isothermally cycled specimens.

The specimens thermomechanically cycled with hold periods were also examined by TEM and characteristic substructures are shown in Figure 12. Most regions of the materials showed some cell formation with many cells having well-ordered dislocation arrays in the walls. These cells tended to be about 0.5 μm in size and, in general, smaller than those developed under continuous thermomechanical cycling conditions.

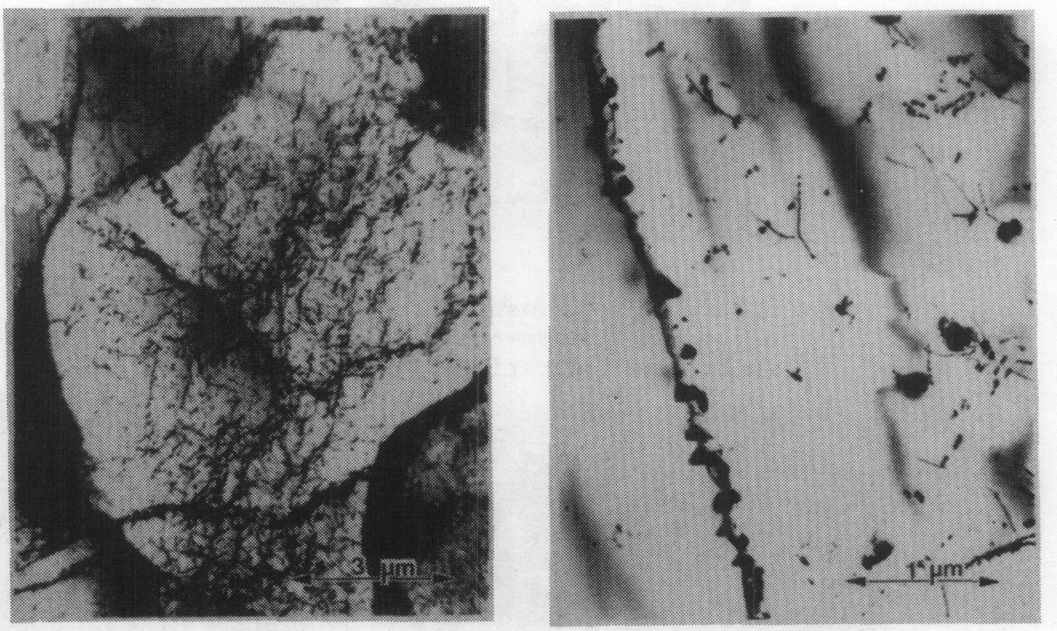

(a) (b)

Figure 10. Transmission electron micrographs of Alloy 800 isothermally cycled at 649°C, 60 s/cycle, 256 hr. test duration.

Figure 11. Transmission electron micrograph of Alloy 800 thermomechanical HTC cycled, 60 s/cycle, 75 hr. test duration.

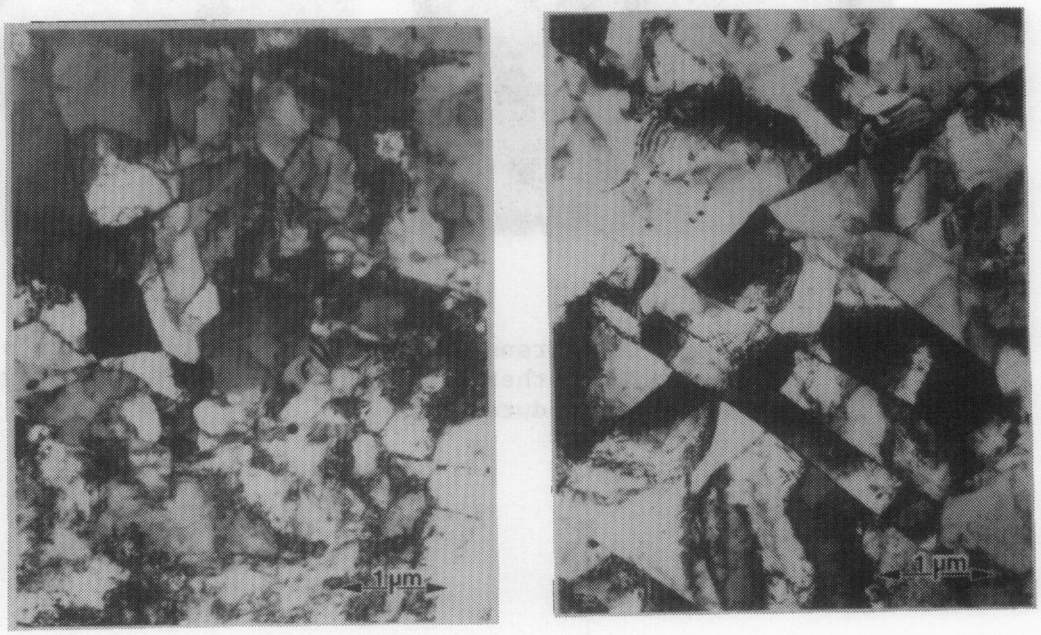

(a) (b)

Figure 12. Transmission electron micrographs of Alloy 800 thermomechanical HTC cycled, 60 s/cycle:
(a) 5 min. tensile hold, 120 hr. test duration;
(b) 5 min. compressive hold, 40 hr. test duration.

The test with a 5 minute compressive (and maximum temperature) hold period failed at 2380 cycles after 40 hours of test and the test with a 5 minute hold period in tension (at the minimum temperature) failed at about 7200 cycles or 120 hours of test. Neither specimen showed any indication of carbide precipitation during testing. This is reasonable given the short time either specimen was exposed to elevated temperature.

Fractographic Observations

Isothermal Testing. Fracture surfaces of 316 Stainless Steel isothermally cycled at 649°C are shown at two different crack lengths in Figure 13. Crack growth occurs by ductile striation formation over the entire surface, with considerable secondary cracking out of the main crack plane also evident. At short crack lengths (<0.75 mm) the surface is obscured by oxidation, and striations are not visible.

Fatigue fracture of Alloy 800 at the same temperature shown in Figure 14 is significantly different. Here cracking proceeds by a mixed mode which is partially intergranular and partially ductile. Blocky features on the surface are comparable to the grain size of 10 - 15 μm. Some striations are visible only over a limited crack length range of 1.0 - 1.6 mm, and these are mixed with the intergranular features.

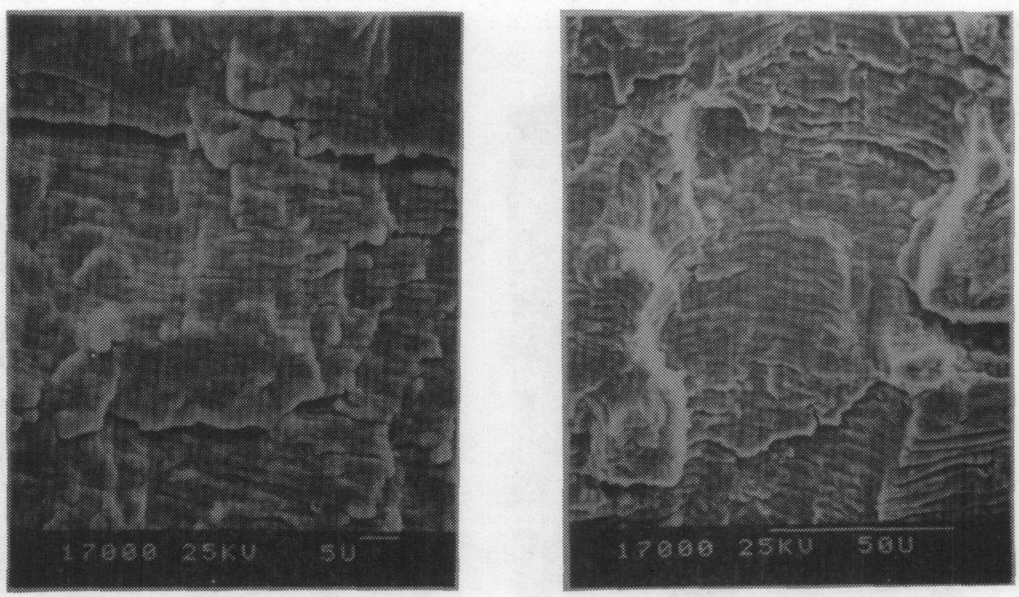

(a) (b)

Figure 13. Fatigue fracture surface of 316 Stainless Steel isothermally cycled at 649°C: (a) crack length = 1.33 mm; (b) crack length = 1.97 mm.

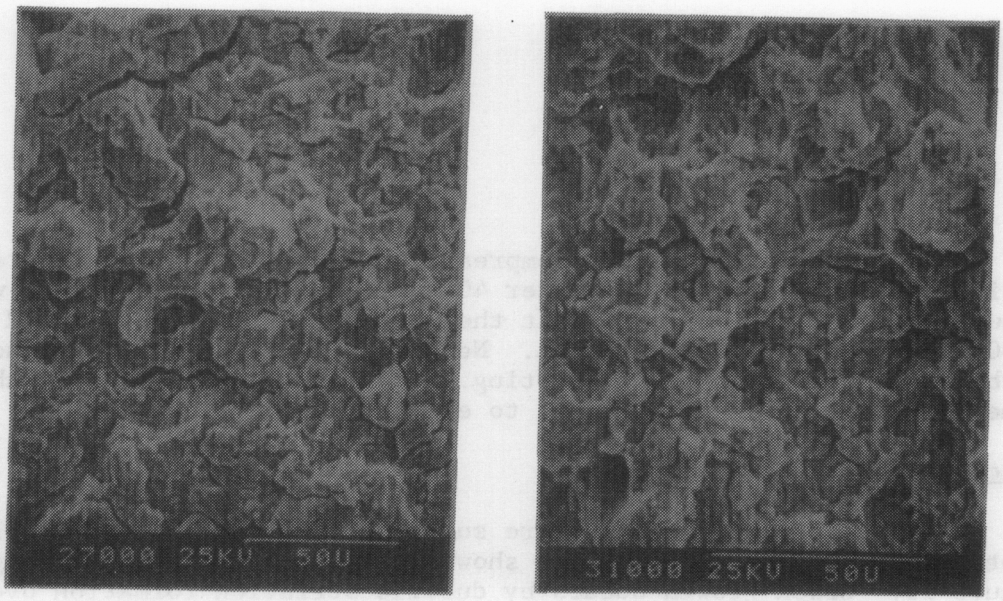

(a) (b)

Figure 14. Fatigue fracture surface of Alloy 800 isothermally cycled at 649°C: (a) crack length = 1.30 mm; (b) crack length = 2.02 mm.

Thermal Fatigue. Cracking of both alloys cycled under HTC conditions occurs by the ductile striation mechanism. Figure 15 shows continuously cycled Alloy 800 and 316 Stainless Steel. Roughly spherical particles on the surface of the Alloy 800 sample are nucleated surface oxide; these grow larger and become closer together at short crack lengths. HTC thermomechanical fatigue tests of Alloy 800 with either 5 minute compressive (5C) or tensile (5T) hold periods also crack by striation formation (Figures 16 and 17).

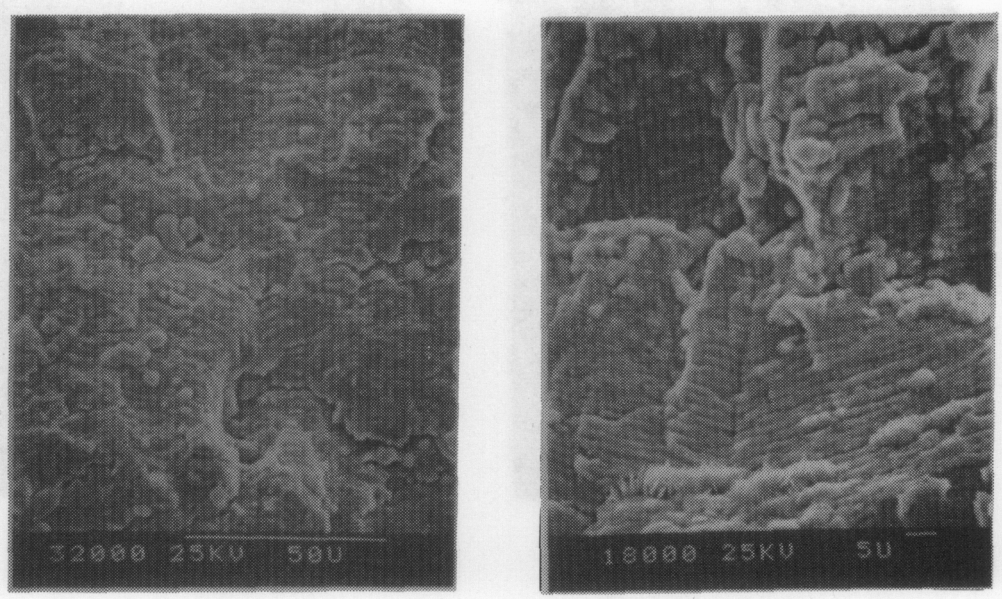

(a) (b)

Figure 15. Fatigue fracture surface of HTC thermomechanical fatigue cycle specimens:
(a) Alloy 800, crack length = 1.00 mm;
(b) 316 Stainless Steel, crack length = 2.22 mm.

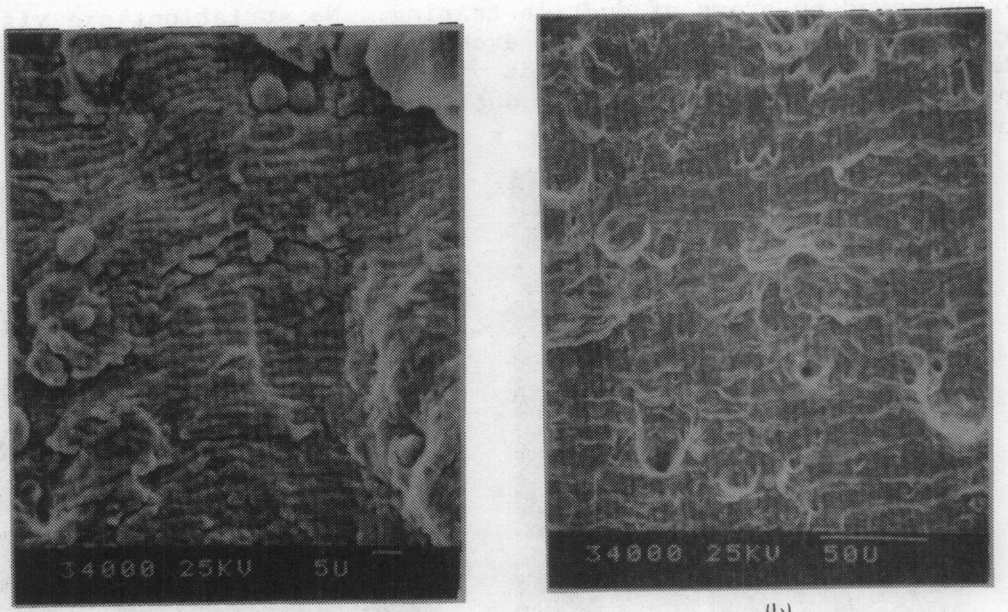

(a) (b)

Figure 16. Fatigue fracture surface of HTC thermomechanical fatigue cycled Alloy 800 with 5 min. compressive hold period: (a) crack length = 0.77 mm; (b) crack length = 2.00 mm.

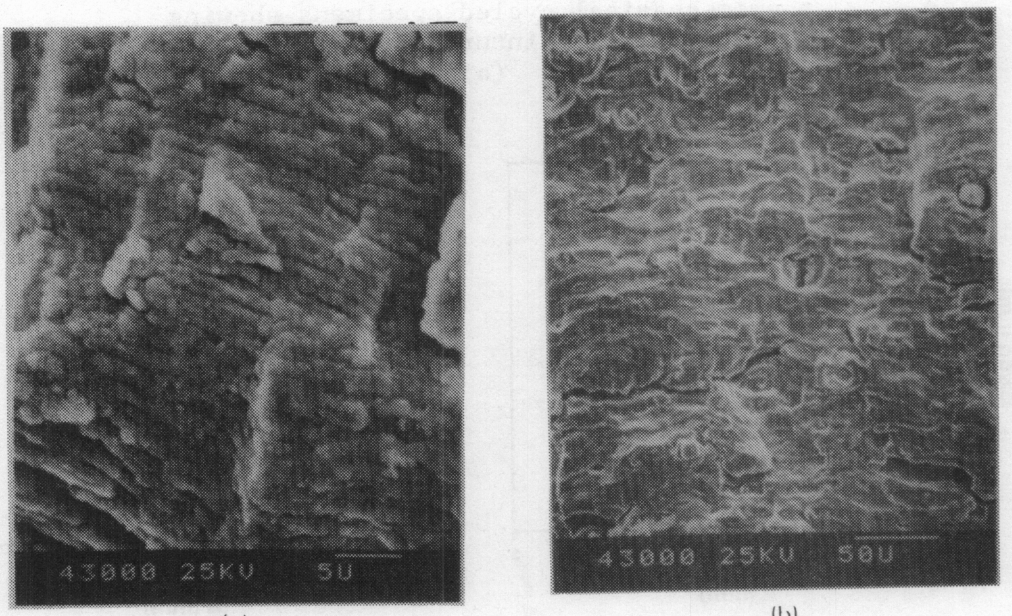

(a) (b)

Figure 17. Fatigue fracture surface of HTC thermomechanical fatigue cycled Alloy 800 with 5 min. tensile hold period: (a) crack length = 0.66 mm; (b) crack length = 2.84 mm.

HTT thermomechanical fatigue produced mixed mode failures in both alloys. For 316 Stainless Steel (Figure 18a), the surface is comprised of several large regions (≃0.3 mm diameter) of intergranular failure which are interconnected by areas of ductile tearing. No striations are visible. Alloy 800 shows similar behavior, except the size scale is different. A few predominantly intergranular islands visible are about 0.1 mm in diameter (Figure 18b) and are separated by ductile tearing with void formation. Again, no striations are visible.

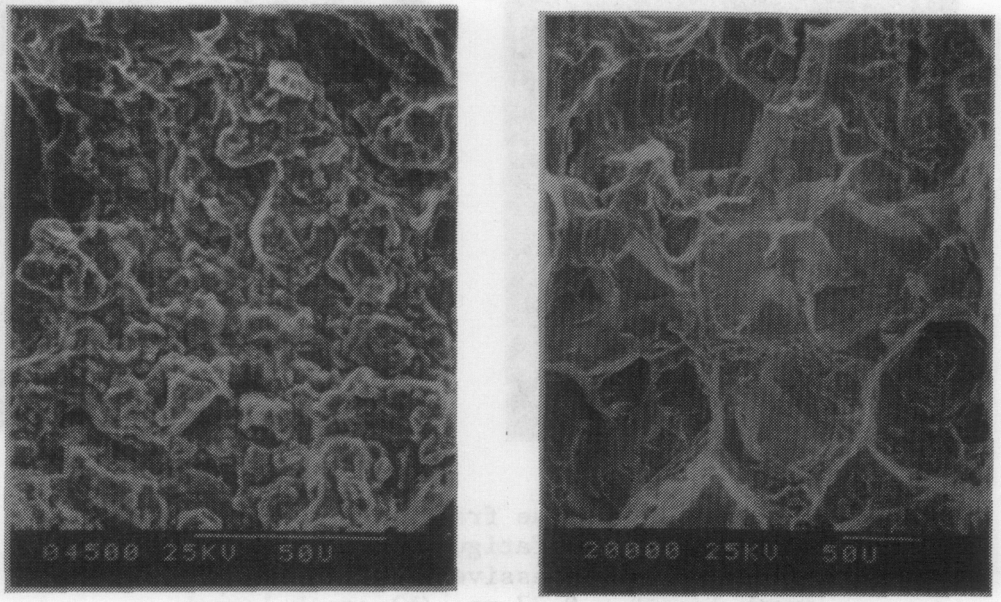

(a) (b)

Figure 18. Fatigue fracture surfaces of HTT themomechanical cycled specimens showing regions of mixed intergranular and intragranular ductile fracture: (a) Alloy 800; (b) 326 Stainless Steel.

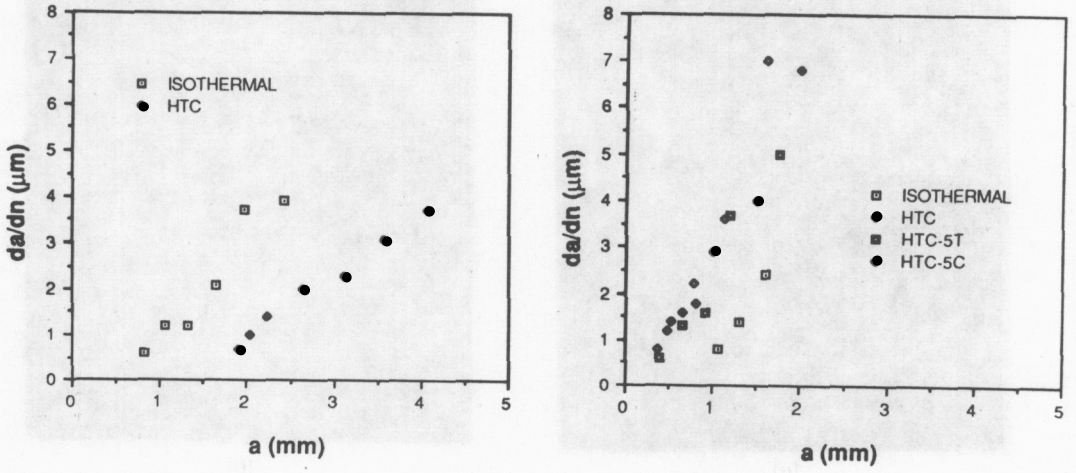

(a) (b)

Figure 19. Striation spacing crack growth rates versus crack length for isothermal and HTC thermomechanical cycling for (a) 316 Stainless Steel and (b) Alloy 800.

Crack Growth Rates. Fatigue crack growth rates measured by striation spacings are shown in Figure 19a and b for the test conditions where distinct striations could be observed. Isothermal tests with long cycle times were too oxidized to view striations, and the HTT thermomechanical fatigue tests did not form striations. With 316 Stainless Steel, growth rates are significantly higher for isothermal cycling than for thermomechanical fatigue HTC loading. Contrary to this, TMF cycling in Alloy 800 produces a higher growth rate than isothermal cycling. The three sets of data for HTC cycling with and without hold times in Alloy 800 are very similar and result in overlapping growth curves. Isothermal growth rates for the two alloys are about the same, but thermomechanical fatigue HTC crack growth in Alloy 800 is faster than in 316 Stainless Steel.

Discussion

The large decrease in cycles-to-failure for TMF is an observation of sizable engineering impact which warrants rationalization and interpretation. The discussion which follows is aimed at examining three possible sources for these observations:

- unique microstructural changes,
- cyclic stress-strain response,
- and their effects on fatigue crack initiation and propagation.

Microstructural Observations

Precipitation of $M_{23}C_6$ carbides during elevated temperature exposure of 316 Stainless Steel has been thoroughly examined under conditions of isothermal aging (11, 12) and in elevated temperature low cycle fatigue (16, 17). The $M_{23}C_6$ carbide is the first phase to form in this steel and is the only phase observed for aging periods of up to 1000 hours at 650°C (11). This aging produces predominantly grain boundary precipitation of large particles and no intragranular precipitation when the starting material was well annealed. Heterogeneous nucleation becomes predominant during low cycle fatigue at elevated temperature (16, 17). These particles form in a distribution reflective of the current dislocation substructure and would essentially lock-in that structure, but the density of these precipitates is not sufficient to alter the flow stress of the alloy (17). The results of this study are consistent with this earlier work.

The effect of thermomechanical cycling on this precipitation process (Figure 9) is to simply retard the formation rate of $M_{23}C_6$, and no unique synergism appears to occur. The TTT (time-temperature-transformation) curve for this reaction (11) indicates that the nose of the curve is at about 800°C so that the thermomechanical cycling in this study encompassed a range fully below the nose of the curve. Lai (12) has shown that the rate of $M_{23}C_6$ precipitation is chromium diffusion controlled in this region. This would suggest that the effect on precipitation kinetics of thermomechanical cycling between 360 and 650°C would only appear through the temperature dependence of chromium diffusivity. Our results are consistent with this rationale. Thermomechanical cycling which extends to higher temperatures above the nose of the TTT-curve may, however, produce different effects. This is a possibility since the controlling mechanism in $M_{23}C_6$ precipitation would be changing over the period of each thermomechanical cycle: from

nucleation controlled at the peak temperature to growth controlled by Cr diffusion at the lower temperatures.

The mechanical strain range was 0.5% in both the isothermal and the thermomechanical cycling tests so that differences in plastic strain range and the dislocation substructures would reflect only the thermal cycling. As Figures 8 and 9 indicate, the differences are minor. The cell walls in the isothermally aged specimens did appear to be generally better ordered, but not uniformly so. There appear to have been competing processes which have combined to produce these fairly similar substructures. The dislocation substructure development for LCF is hindered by the precipitation of the intragranular $M_{23}C_6$ particles. Because of this distribution of hard precipitate particles, a well developed subgrain structure cannot develop during continuous cycling even though the temperature is high enough to facilitate the necessary climb to produce a well ordered subgrain structure. The limiting features under thermomechanical cycling conditions are different. Since dislocation climb is more difficult at the lower temperatures, thermomechanical cycling would not be expected to give rise to a well ordered substructure. Climb and dislocation annihilation processes cannot proceed at the cool end of the thermomechanical cycles so that dislocation tangling and multiplication would occur. The final structure then reflects some climb and annihilation by dislocations at the higher temperatures but also reflects the dislocation multiplication and tangling going on at lower temperatures.

For Alloy 800, as with 316 Stainless Steel, precipitation of $M_{23}C_6$ is the dominant precipitation process at temperatures below 650°C. Comparison of Figures 10 and 11 show microstructural evolution effects similar to those just discussed for 316 Stainless Steel. Intragranular precipitation similar to that shown in Figure 10 of $M_{23}C_6$ in Alloy 800 during elevated creep and fatigue has been observed earlier (8, 13, 18). The approximate TTT-curve given by Jones (9) for $M_{23}C_6$ formation indicates a maximum precipitation rate at about 720°C which is above the peak temperature used in this study. The available carbon in the starting matrix of this heat of material is sufficient to produce subsequent precipitation, both intragranularly and intergranularly, in the isothermally cycled specimen (Figure 10). This precipitation has not occurred in the thermomechanically cycled specimen (Figure 11) during the time of the test. Here again, the precipitation rate is controlled by diffusion, probably chromium, and the thermomechanical cycling slows the precipitation kinetics accordingly. Had the thermomechanical cycling test continued, the $M_{23}C_6$ carbide would have formed after longer times. Similar arguments apply to the microstructures developed in thermomechanical cycling with hold periods shown in Figure 12. The total time at high temperature was insufficient to result in $M_{23}C_6$ formation.

The carbide precipitation in the isothermal test of Alloy 800 appears to have influenced the dislocation substructure development. This can be seen by comparing Figures 10 and 11. As was observed in 316 Stainless Steel, the fine distribution of carbides hindered the development of a clean cell structure. The thermomechanically cycled material showed a cleaner cell structure in spite of the large fraction of time spent at lower temperatures. The specimen which was subjected to a 5 minute hold period at the peak temperature (compressive strain peak) developed the clearest

subgrain structure with narrow, low angle boundaries. The specimen in Figure 12 was held at the minimum temperature for 5 minutes and the dislocation substructure is very similar to that formed during continuous cycling TMF. These are consistent with the time-temperature histories of those tests.

The γ' phase was not observed in any of the Alloy 800 specimens, although this heat of Alloy 800 is known to form γ' under isothermal aging at 649°C (9). An earlier study (8) involving isothermal cycling at 565°C, where a larger volume fraction of γ' is stable, did show its formation during cycling. Fewer and extensively cut γ' particles were present for the LCF history than for the isothermal aging. The results at 649°C from this study indicate that the precipitate cutting followed by resolution which occurs during cycling effectively precludes γ' formation during any kind of mechanical cycling.

In summary, no unique synergism between TMF and microstructural development appears to have occurred for either 316 Stainless Steel or Alloy 800. Both the carbide precipitation and dislocation substructure evolution reflect the slowing of both solute and vacancy diffusion which takes place as the temperature is decreased below 649°C. Nothing was observed to indicate that either carbide morphology or dislocation substructure differences contribute significantly to the difference in cycles-to-failure observed between LCF and TMF histories.

Cyclic Hardening

Two principal observations may be made regarding the cyclic hardening response of 316 Stainless Steel and Alloy 800: both alloys develop mean stresses during thermomechanical cycling and both quantitative and qualitative differences exist in the cyclic development of these mean stresses. Two separate macroscopic mechanisms may be invoked to explain the continuous cycling stress asymmetry, the combined effect of which may also explain the differing response of the two alloys.

The first contribution to mean stress development is the influence of temperature on the plastic constitutive relationships for these alloys. Both 316 Stainless Steel and Alloy 800 exhibit a dependence of yield stress and cyclic strain hardening within the temperature range of our TMF tests (19), the result of which is, in general, a slight decrease in flow stress with increasing temperature. As part of a companion study of 304 stainless steel (20), calculations simulating TMF have been performed using a temperature dependent, elastic-plastic constitutive model. It has been shown that TMF of a material displaying such temperature dependent deformation can result in the development of mean stresses on the low temperature side of the cycle, as is shown by both 316 Stainless Steel and Alloy 800. Thus mean stress development can be explained by evoking a simple dependence of plastic flow on temperature.

The second contribution to mean stress development is the character of viscous flow in these two alloys. Previous work can be examined to conclude that time dependent flow is more important during cyclic loading for Alloy 800 than for 316 Stainless Steel. Isothermal low cycle fatigue tests have been performed by Jones (21) at 649°C with 5 minute compressive holds for

both alloys. It was seen that Alloy 800 shows approximately three times the level of stress relaxation that was displayed by 316 Stainless Steel. Also, Alloy 800 develops significant tensile mean stresses during hold time cycling, while 316 Stainless Steel does not. Thus one can expect that Alloy 800 would show more structural relaxation during the high temperature end of the TMF cycle than 316 Stainless Steel, resulting in enhanced mean stress development on cooling and reversed straining. This is supported by the observation that incorporating a five minute compressive hold in the HTC thermomechanical fatigue testing of Alloy 800 results in exaggerated mean stress development similar to that shown in continuous cycling.

The combination of these two effects would lead to mean stress development in both alloys with an exaggerated effect in Alloy 800, which is consistent with the observations of this study. We have not determined the micromechanism by which these two alloys differ. It can be deduced that the differences are subtle since the substructures are so similar. This issue is the subject of continuing work. In summary, the development of significant tensile mean stresses under TMF conditions would be expected to contribute to a loss of fatigue life through either or both crack nucleation or growth.

Fractography

The fatigue fracture modes of this category of austenitic alloys are well known to be temperature and strain rate dependent (22, 23, 24). At lower temperatures or high rates, propagation by ductile striations dominates, while at elevated temperatures intergranular cracking will occur at slow strain rates or with tensile hold periods. Results for the isothermal tests at 649°C and 10 s/cycle show that 316 Stainless Steel is still in the ductile regime while Alloy 800 is mixed mode with combined ductile striation and intergranular cracking. For HTC thermomechanical cycling where the peak tensile loads are at the low temperature extreme of the thermomechanical cycle (360°C), crack advance occurs at low temperature by ductile striation formation. Thus for Alloy 800 the mode is shifted to the ductile mode even for the hold period tests.

In the HTT tests of both alloys, maximum tensile loading and crack advance occur at the peak temperature of the thermomechanical cycle. Both alloys failed in mixed mode where intergranular fracture formed as island-like regions separated by ductile tearing. This suggests that the lower strain rate of these 60 s/cycle tests promotes intergranular fracture and that the intergranular regions nucleated ahead of the main crack front. This mode change did not significantly affect the total cycles to failure for either alloy.

Fatigue Life

It is possible to calculate the number of cycles spent in propagating a fatigue crack across each specimen by integrating the crack growth data given in Figure 20. This was done using a numerical approximation where the growth rate between any two adjacent crack length intervals was taken as the average of the rates at the beginning and end of the interval. Final crack lengths were measured for each sample, and an initial growth rate equal to

the measured rate at the shortest observable crack length was assumed from initiation to that length. This last assumption may cause the calculation to somewhat underestimate the number of propagation cycles for small crack lengths. Errors of even 150% in this calculation would not affect the overall conclusions.

Calculated values of cycles spent in crack propagation and, by subtraction, cycles for crack initiation are given in Table 4 along with values of total fatigue life for the particular specimens examined. For 316 Stainless Steel in isothermal cycling, about 15% of the fatigue life is spent in crack propagation, requiring 85% for the initiation process. This fraction is similar to previous measurements at an equivalent strain range at 593°C on 316 Stainless Steel (25) and 304 Stainless Steel (26). Isothermal cycling in Alloy 800 did not yield striations over enough of the crack length to allow the propagation calculations, but the limited rates measured (Figure 20b) are comparable to 316 Stainless Steel. Again, earlier measurements of Alloy 800 at 565°C and 0.5% total strain range showed propagation by ductile striations and approximately 90% of life spent in crack initiation (27). This would imply that the propagation cycles here are a small fraction of the total for isothermally cycled Alloy 800.

Table 4 - Cycles for Crack Propagation and Total Cycles to Failure

Material	Test Type	Cycles in Propagation	Total Cycles	Cycles in Initiation*
316	isothermal, 649°C	3100	21514	18400
316	thermal/HTC	4300	7060	2800
800	isothermal, 649°C	---	110000	≃100000
800	thermal/HTC	1100	4500	3400
800	thermal/HTC/5C	1000	2418	1400
800	thermal/HTC/5T	1500	7300	5800

*Approximate based on Nt = Ni + Np

Crack initiation arguments can be used to explain the large difference in fatigue life between the two alloys in isothermal cycling (Table 3). Taira, et al (28) showed that cycles to microcrack initiation decreases with increasing grain size for a ferritic low carbon steel. Essmann et al (29) and Mughrabi et al (30) relate this to diminished surface intrusion and extrusion formation for smaller grain material. Intrusions and extrusions form as a result of localized dislocation slip intersecting the sample surface as persistent slip bands (PSB's); microcracks can initiate at PSB's with large height or slip offset. The height of PSB's decreases with shorter slip distance to the nearest grain boundary, so PSB height and microcrack formation are less for small grain material. Cheng and Laird (31) experimentally showed that PSB height increases with plastic strain amplitude in copper crystals and from this derived a model which showed that cycles to initiation decreases with increasing PSB offset. Given that the measured isothermal cyclic stress-strain hardening responses of small grain Alloy 800 and large grain 316 Stainless Steel are nearly identical, leading

to equal plastic strain ranges, the grain size effect on crack initiation likely accounts for the large difference in total isothermal life of the alloys.

Fractions of life spent in propagation during HTC cycling range from 20 to 40% for Alloy 800 samples to 60% for 316 Stainless Steel (Table 4). These relative fractions are much greater than for isothermal cycling at 649°C. Cycles for propagation of Alloy 800 for continuous and 5 minute hold period thermomechanical fatigue tests are similar, within the uncertainties of the method. The large drop in life for 316 Stainless Steel is accompanied by an equal or greater number of cycles for propagation.

These data clearly show that crack propagation effects also cannot be used to explain the large decreases in fatigue life observed with TMF cycling, since propagation does not dominate the total life at this strain range. By deduction, this study suggests that crack initiation also dominates the TMF response. One possibility was that the experimental technique itself might give rise to surface thermal stresses leading to early crack initiation. The analysis described in the Experimental Procedures section shows this to be unlikely.

The initiation process in TMF cycling occurs under significantly different mechanical and thermal conditions from the isothermal case. In addition, results also indicate that the grain size differences between the two alloys does not significantly influence failure rates. Much of the plastic deformation in the loading cycle takes place at lower temperatures, where it is expected that athermal deformation processes would dominate. This could tend to limit thermally activated climb and cross-slip processes, thus promoting more planar slip which would favor PSB formation. TEM surveys of the bulk did not show a strong tendency toward planar slip, and closer examination of surface deformation features is required. As shown earlier, stress range is greater and plastic strain range is smaller in TMF cycling. Cheng and Laird's model for initiation (31) based on PSB formation predicts that lower strain range would lead to delayed crack initiation, which was not observed here. This suggests that higher stress, independent of plastic strain range, is significant, but at this time it is difficult to completely assess its effects. Higher stresses could increase the number of dislocations piled up at grain boundaries, allowing more offset at the surface. Conversely, higher resolved stress on slip planes could lead to increased cross-slip and more diffuse slip lines; this would favor less concentrated PSB's and delayed initiation. To sort out these possible effects, additional work is continuing to directly observe the initiation processes and relate them to near surface deformation features during TMF cycling.

Conclusions

1. TMF between 649 and 360°C shortens the fatigue life of both 316 Stainless Steel and Alloy 800 when compared to LCF at 649°C at a strain range of 0.5%. This loss of fatigue life is more marked in Alloy 800 than for 316 Stainless Steel. In both alloys, this effect must be considered in the design of structures which see thermal cycling in service.

2. This TMF cycling does not produce any unique synergisms in either the precipitate or dislocation substructures. The $M_{23}C_6$ carbide formed in both alloys during LCF but not during TMF for the duration of testing in this study. Dislocation cell structures were incompletely developed in the LCF samples due to intragranular $M_{23}C_6$ precipitation and in the TMF samples due to the difficulty of recovery at the low temperature end of each cycle.

3. Mean stresses are developed by both alloys under TMF conditions. These are larger for Alloy 800 than for 316 Stainless Steel with the HTC cycle producing tensile mean stresses. Differences in time-dependent flow characteristics between these alloys produce this effect.

4. Fractographic analysis has shown that TMF accelerates fatigue crack growth in Alloy 800 and may slightly retard crack growth in 316 Stainless Steel. In both alloys, cracking occurs by a ductile striation mechanism. Under LCF conditions, 316 Stainless Steel showed ductile striations while Alloy 800 showed a mixture of intergranular and ductile intragranular modes.

Acknowledgements

The authors acknowledge the assistance of D. T. Schmale in the development of the TMF test system and of C. R. Hills in the transmission electron microscopy.

References

1. H. Sehitoglu, "Characterization of Thermomechanical Fatigue," pp 93-110 in Thermal and Environmental Effects in Fatigue: Research/Design Interface, ASME, New York, 1983.

2. J. Ginsztler, "Assessment of Thermal Fatigue Resistance of Some Boiler Steels," pp 335-338 in Pressure Vessel Technology, Vol. 1, Inst. of Mech. Engrs., London, 1980.

3. D. J. Marsh, "A Thermal Shock Fatigue Study of Type 304 and 316 Stainless Steels," Fatigue Eng. Mater. Struct., 4 (1981) pp 179-195.

4. J. B. Conway, J. T. Berling, and R. H. Stentz, "Low-Cycle Fatigue and Cyclic Stress-Strain Behavior of Incoloy 800," Met. Trans, 3 (1972) pp 1633-1637.

5. D. R. Diercks, "A Compilation of Elevated-Temperature, Strain-Controlled Fatigue Data on Type 316 Stainless Steel," Argonne National Laboratory Report ANL/MSD-77-8, 1978.

6. S. Majumdar, "Compilation of Fatigue Data for Incoloy 800 Alloys," Argonne National Laboratory Report ANL/MSD-78-3, 1978.

7. J. Orr, "A Review of the Structural Characteristics of Alloy 800," pp 25-60 in Alloy 800, W. Betteridge, et al, eds.; North-Holland Publishing Company, New York, 1978.

8. W. B. Jones and R. M. Allen, "Mechanical Behavior of Alloy 800 at 838 K," Met. Trans. A, 13A (1982) pp 637-648.

9. W. B. Jones, "Creep-Fatigue and Temperature Synergisms in Alloy 800," pp 403-418 in Fracture: Interactions of Microstructure, Mechanisms and Mechanics, J. M. Wells and J. D. Landes, eds., AIME, New York, 1984.

10. A. H. Nahm and J. Moteff, "Characterization of Fatigue Substructure of Incoloy Alloy 800 at Elevated Temperature, Met. Trans. A, 12A (1981) pp 1011-1025.

11. B. Weiss and R. Stickler, "Phase Instabilities During High Temperature Exposure of 316 Austenitic Stainless Steel," Met. Trans., 3 (1972) pp 851-865.

12. J. K. L. Lai, "A Study of Precipitation in AISI Type 316 Stainless Steel." Mater. Sci. and Eng., 58 (1983) pp 195-209.

13. H. Nahm and J. Moteff, "Second Phase Formation and its Influence on the Fatigue Properties of Incoloy 800 at Elevated Temperatures," Met. Trans A., 7A (1976) pp 1473-1477.

14. D. T. Schmale and R. W. Cross, "Techniques for Elevated Temperature Mechanical Testing," Sandia National Laboratories Report SAND82-0727 (NUREG/CR-2793, 1982.

15. M. D. Mikhailov and Ozisik, Unified Analysis and Solutions of Heat and Mass Diffusion, pp 305-318, Wiley Interscience Publishers, New York, 1984.

16. K. D. Challenger and J. Moteff, "Correlation of Substructure with the Elevated Temperature Low-Cycle Fatigue of AISI 304 and 316 Stainless Steels," in Fatigue at Elevated Temperatures, ASTM STP 520, A. E. Carden, et al, eds., ASTM, Philadelphia, 1973.

17. E. R. De Los Rios and M. W. Brown, "Cyclic Strain Hardening of 316 Stainless Steel at Elevated Temperatures," Fatigue Eng. Mater. Struct., 4 (1981) pp 377-388.

18. A. Orlova, K Milicka, and J. Cadek, "Precipitation of Intragranular $M_{23}C_6$ Particles and their Effect on the High Temperature Creep of Austenite," Mat. Sci and Eng., 50 (1981) pp 221-227.

19. P. S. Maiya, "Cyclic Stress-Strain Curves and Cyclic-Hardening Behavior for Types 304 and 316 Stainless Steel and Incoloy Alloy 800H," Argonne National Laboratory Report ANL-80-100, 1980.

20. R. J. Bourcier, "Numerical Simulation of the Thermal Fatigue of 304 Stainless Steel," presented at 1986 AIME Fall Meeting, Orlando, FL, October 1986.

21. W. B. Jones, unpublished research, 1987.

22. D. J. Michel and H. H. Smith, "Accelerated Creep-Fatigue Crack Propagation in Thermally Aged Type 316 Stainless Steel," Acta Metallurgica, 28 (1981), pp 999-1007.

23. S. Taira, R. Ohtani, and T. Komatsu, "Application of J-Integral to High-Temperature Crack Propagation, Part II -- Fatigue Crack Propagation," Journal of Engineering Materials and Technology, Vol. 101, pp 162-167.

24. J. Wareing, H. G. Vaughan, and B. Tomkins, "Mechanisms of Elevated-Temperature Fatigue Failure in Type 316 Stainless Steel," UKAEA ND-R-447(S), September 1980.

25. J. A. Van Den Avyle, "Low Cycle Fatigue of Tubular Specimens," Scripta Metallurgica, Vol. 17, pp 737-740.

26. P. S. Maiya, in "Mechanical Properties Test Data for Structural Materials, Quarterly Progress Report for Period Ending January 31, 1975," ORNL-5104, 1975, p 13.

27. J. A. Van Den Avyle, "Fatigue Crack Growth Under Fully Plastic Cycling in 316 Stainless Steel and Alloy 800," to be published.

28. S. Taira, K. Tanaka, and M. Hoshima, "Grain Size Effect on Crack Nucleation and Growth in Long-Life Fatigue of Low-Carbon Steel," Fatigue Mechanisms, ASTM STP 675, 1979, pp 135-173.

29. U. Essmann, U. Gosele, and H. Mughrabi, "A Model of Extrusion and Intrusions in Fatigued Metals; Part 1: Point Defect Production and Growth of Extrusions," Philosophical Magazine A, Vol. 44, 1981, pp 405-426.

30. H. Mughrabi, R. Wang, K. Differt, and U. Essmann, "Fatigue Crack Initiation by Cyclic Slip Irreversibilities in High Cycle Fatigue," Fatigue Mechanisms: Advances in Quantitative Measurement of Physical Damage, ASTM STP 811, 1983, pp 5-45.

31. A. S. Cheng and C. Laird, "Fatigue Life Behavior of Copper Single Crystals, Parts 1 and 2," Fatigue of Engineering Materials and Structures, Vol. 4, 1982, pp 331-341 and 343-353.

Distribution:

Analysis Review & Critique
6503 81st Street
Cabin John, MD 20818
Attn: C. LaPorta

Arizona Public Service Company
P.O. Box 21666
Phoenix, AZ 85036
Attn: E. Weber

Babcock and Wilcox
91 Stirling Avenue
Barberton, OH 44203
Attn: D. Young

Bechtel Group, Inc.
P.O. Box 3965
San Francisco, CA 94119
Attn: P. DeLaquil
S. Fleming

Black & Veatch Consulting Engineers (2)
P.O. Box 8405
Kansas City, MO 64114
Attn: J. C. Grosskreutz
J. E. Harder

Boeing Aerospace
Mail Stop JA-83
P.O. Box 1470
Huntsville, AL 35807
Attn: W. D. Beverly

California Energy Commission
1516 Ninth Street, M/S 40
Sacramento, CA 95814
Attn: A. Jenkins

California Public Utilities Com.
Resource Branch, Room 5198
455 Golden Gate Avenue
San Francisco, CA 94102
Attn: T. Thompson

Centro Investigations Energetica
Medroansental Technologie (CIEMAT)
Avda. Complutense, 22
28040 Madrid
SPAIN
Attn: F. Sanchez

DFVLR EN-TT
Institute for Technical Thermodynamics
Pfaffenwaldring 38-40
7000 Stuttgart 80
Federal Republic of Germany
Attn: Dr. Manfred Becker

El Paso Electric Company
P.O. Box 982
El Paso, TX 79946
Attn: J. E. Brown

Electric Power Research Institute (2)
P.O. Box 10412
Palo Alto, CA 94303
Attn: J. Bigger
E. DeMeo

Foster Wheeler Solar Development Corporation
12 Peach Tree Hill Road
Livingston, NJ 07039
Attn: S. F. Wu

Georgia Institute of Technology
GTRI/EMSL Solar Site
Atlanta, GA 30332

D. Gorman
5031 W. Red Rock Drive
Larkspur, CO 80118

Jet Propulsion Laboratory
4800 Oak Grove Drive
Pasadena, CA 91103
Attn: M. Alper

Los Angeles Department of Water and Power
Alternate Energy Systems
Room 661A
111 North Hope Street
Los Angeles, CA 90012
Attn: Hung Ben Chu

Martin Marietta Aerospace
P.O. Box 179, MS L0450
Denver, CO 80201
Attn: H. Wroton

McDonnell Douglas (2)
MS 49-2
5301 Bolsa Avenue
Huntington Beach, CA 92647
Attn: R. L. Gervais
J. E. Raetz

Meridian Corporation
5113 Leesburg Pike
Falls Church, VA 22041
Attn: D. Kumar

Public Service Company of New Mexico
M/S 0160
Alvarado Square
Albuquerque, NM 87158
Attn: T. Ussery
A. Martinez

Olin Chemicals Group (2)
120 Long Ridge Road
Stamford, CT 06904
Attn: J. Floyd
D. A. Csejka

Pacific Gas and Electric Company (4)
3400 Crow Canyon Road
San Ramon, CA 94526
Attn: G. Braun
T. Hillesland
B. Norris
C. Weinberg

Public Service Company of Colorado
System Planning
5909 E 38th Avenue
Denver, CO 80207
Attn: D. Smith

Rockwell International
Rocketdyne Division
6633 Canoga Avenue
Canoga Park, CA 91304
Attn: J. Friefeld

Sandia Solar One Office
P.O. Box 366
Daggett, CA 92327
Attn: A. Snedeker

Science Applications International Corporation
10401 Roselle Street
San Diego, CA 92121
Attn: B. Butler

Solar Energy Research Institute (3)
1617 Cole Boulevard
Golden, CO 80401
Attn: B. Gupta
D. Hawkins
L. M. Murphy

Solar Kinetics, Inc.
P.O. Box 47045
Dallas, TX 75247
Attn: J. A. Hutchison

Southern California Edison
P.O. Box 325
Daggett, CA 92327
Attn: C. Lopez

Stearns Catalytic Corporation
P.O. Box 5888
Denver, CO 80217
Attn: T. E. Olson

Stone and Webster Engineering Corporation
P.O. Box 1214
Boston, MA 02107
Attn: R. W. Kuhr

U.S. Department of Energy (5)
Forrestal Building
Code CE-314
1000 Independence Avenue, SW
Washington, DC 20585
Attn: H. Coleman
S. Gronich
F. Morse
M. Scheve
R. Shivers

U.S. Department of Energy
Forrestal Building
Code CE-33
1000 Independence Avenue, SW
Washington, DC 20585
Attn: C. Carwile

U.S. Department of Energy
Albuquerque Operations Office
P.O. Box 5400
Albuquerque, NM 87115
Attn: D. Graves

U.S. Department of Energy
San Francisco Operations Office
f1333 Broadway
Oakland, CA 94612
Attn: R. Hughey

University of California
Environmental Science and Engineering
Los Angeles, CA 90024
Attn: R. G. Lindberg

University of Houston (2)
Solar Energy Laboratory
4800 Calhoun
Houston, TX 77704
Attn: A. F. Hildebrandt
L. Vant-Hull

1522 R. D. Krieg
1800 R. L. Schwoebel
1820 R. E. Whan
1822 K. H. Eckelmeyer
1830 M. J. Davis
1832 W. B. Jones (10)
1832 R. J. Bourcier (10)
1832 D. R. Frear
1832 D. T. Schmale
1832 J. A. VanDenAvyle (10)
3141 S. A. Landenberger (5)
3151 W. L. Garner (3)
3154-1 C. H. Dalin (28)
For DOE/OSTI
6000 D. L. Hartley
6200 V. L. Dugan
6220 D. G. Schueler
6222 J. V. Otts (4)
6226 J. T. Holmes (10)
8000 R. S. Claassen
8524 P. W. Dean
8100 E. E. Ives
8130 J. D. Gilson
8133 A. C. Skinrood